# Extended-State-Observer-Based Adaptive Prescribed Performance Control for Hydraulic Systems With Full-State Constraints

Zhangbao Xu, Wenxiang Deng, Hao Shen, *Member, IEEE*, and Jianyong Yao, *Member, IEEE*

***Abstract*—In this article, an innovative backstepping controller for hydraulic systems is proposed to handle system uncertainties and accomplish specified performance tracking without violating the full-state constraints. To deal with uncertainties, extended state observers ESOs and an adaptive law are integrated. ESOs are structured to estimate disturbances, whereas adaptive law is applied to approximate unknown parameters. The estimated uncertainties are then incorporated into a constrained controller, ensuring that both the prescribed transient tracking performance and the nonviolation of full-state constraints can be guaranteed. A prescribed performance function (PPF) and the barrier Lyapunov function (BLF) are synthesized to guarantee the transient behavior of the tracking error and all state errors within desirable boundaries. Then, an adaptive prescribed performance controller with uncertainty compensation is constructed by merging the BLF and PPF through backstepping design to stabilize the closed-loop system. Finally, abundant comparative experimental results validate the proposed controller's tracking performance.**

***Index Terms*—Adaptive control, extended state observer (ESO), full-state constraint, hydraulic systems, prescribed performance control.**

## I. Introduction

HYDRAULIC servo systems are extensively used in industries owing to their big load capacity [1]–[4]. Nevertheless, heavy nonlinear behaviors [1], uncertainties [2]–[3], dead-zones [5], constraints [6], saturation [7], etc., make it laborious to exploit closed-loop controllers with excellent performance. In recent years, many sophisticated controllers have been carried out to solve uncertainties (including uncertain nonlinearities and parametric uncertainties) of hydraulic systems and meet the increasingly stringent control performance requirements. To compensate for parametric uncertainties, adaptive control methods [8]–[10] have been developed. However, uncertain nonlinearities, including modeling errors and disturbances, cannot be handled by adaptive controllers. In some cases, when uncertain nonlinearities develop into the primary element affecting the control performance, the tracking accuracy of the system may not be assured. To increase the robustness of adaptive control and improve tracking performance, robust and adaptive controls are usually integrated to deal with uncertainties. Robust adaptive control [11], RISE-based adaptive control [2], [12], [13], adaptive sliding mode control [14], neural network control [15]–[17], and adaptive robust control [3]–[4], [18]–[20] are some of the control algorithms that have been created and applied to hydraulic systems. However, high-gain feedback was realized to be adopted by these controllers for achieving quality performance. In practical systems, high-gain feedback is often avoided regarding its high-frequency dynamic characteristics and measurement noise. As a result, the control strategy is firmly conservative when the system is subjected to large disturbances [21].

In order to enhance the antidisturbance ability, various antidisturbance strategies have been developed [22], [23]. Because disturbance observers are easy to be combined with various control methods, a variety of disturbance observers are used to improve the control performance of hydraulic systems [24]–[26]. These disturbance compensation controllers consider parametric uncertainties and disturbances as lump disturbances that can be estimated by a disturbance observer and then compensated by a feed-forward controller, removing the impact of uncertainties on the systems without using high-gain feedback. Especially in [26], the extended state observer (ESO), proposed by Han [27], could perform disturbance estimation and did not require too much model information. The most important feature is that it only has few parameters and is easy to adjust. Therefore, ESO have been extensively utilized [28]–[31]. However, these controllers do not consider state constraint of hydraulic systems.

Manuscript received 18 April 2022; accepted 5 June 2022. Recommended by Technical Editor D. Chen and Senior Editor Y. Li. This work was supported in part by Natural Science Foundation of the Higher Education Institutions of Anhui Province under Grant KJ2021A0409, in part by Anhui Science and Technology Major Project under Grant 201903a05020029, and in part by the National Nature Science Foundation of China under Grant 52075262. *(Corresponding author: Jianyong Yao.)*

Zhangbao Xu is with the School of Mechanical Engineering, Anhui University of Technology, Maanshan 243002, China (e-mail: xuzhangbao1988@163.com).

Wenxiang Deng is with the School of Mechanical Engineering, Nanjing University of Science and Technology, Nanjing 210094, China (e-mail: wxdeng_njust@163.com).

Hao Shen is with the School of Electrical and Information Engineering, Anhui University of Technology, Maanshan 243002, China (e-mail: haoshen10@gmail.com).

Jianyong Yao is with the School of Mechanical Engineering, Nanjing University of Science and Technology, Nanjing 210094, China (e-mail: jerryyao.buaa@gmail.com).

Color versions of one or more figures in this article are available at https://doi.org/10.1109/TMECH.2022.3186390.

Digital Object Identifier 10.1109/TMECH.2022.3186390

It is necessary to consider the maintenance of states and output constraints in practical applications due to the recent need to maintain ideal dynamic behavior under different uncertainties and disturbances. Tee *et al.* [32] established a technique for preventing constraint violation using the barrier Lyapunov function (BLF) instead of the quadratic Lyapunov function. Subsequently, the BLF is utilized in manipulators and rehabilitation robots [33], [34]. Then, Won *et al.* [24] designed a backstepping controller based on a high-gain disturbance observer using the BLF, which realized the quality control performance of hydraulic systems with constraint to no other state, but the output state. Moreover, state-constrained control is proposed in [35] for the single-rod hydraulic actuators to constrain the states in the channels without disturbances. However, state constraint control in the channels with disturbances is still a challenge that needs to be solved. Then, the BLF is integrated with uncertainties compensation control to achieve nonviolation of all state constraints [6]. Although aforementioned control methods all ensure the global stability of hydraulic systems and achieve good steady-state tracking performance, the transient performance has not been discussed and is ambiguous.

In practical engineering, it is expected that the proposed controller ensures that the system control performance indices (including overshoot, steady-state tracking error, and convergence speed) should meet the actual performance demands. However, insufficient attention is paid to the system transient tracking performance, although the above controllers can guarantee good steady-state control performance. Recently, a prescribed performance control (PPC) proposed in [36] and [37] is used to make the tracking error converge to a prescribed arbitrary small region. First, a new transformed error is obtained from the tracking error of the original system by utilizing the prescribed performance function (PPF). This transformed error is then employed to develop controller. When the controller can stabilize the transformation system, the tracking error of the original system will be remained within a specified range. A few applications of this PPC method for hydraulic systems are presented in [38] and [39]. Nevertheless, it is discovered that PPC has not been employed for tracking control for hydraulic systems with full-state constraints.

Most hydraulic driving systems (such as hydraulic robots) have physical constraints, such as velocity and acceleration constraints. The changes of system's attitude and load may violate these inherent physical constraints, thus severely affecting the control performance. Moreover, fast response and accurate steady-state tracking have often been the pursuit of high-performance control of hydraulic systems. Therefore, for hydraulic systems with uncertainties and full-state constraints, a backstepping controller is designed in this article to enhance the dynamic behavior and steady accuracy. To eliminate system uncertainties, ESOs and adaptive control are integrating. The ESOs are adopted to accurately estimate the matched and mismatched disturbances accurately, and an adaptive law is designed for parametric uncertainties. The estimated uncertainties are then incorporated into a constrained controller such that the prescribed tracking performance and full-state constraints can be assured. The PPF and BLF are combined to realize the prescribed tracking performance and constrain the all system state by constraining the control errors in the corresponding desired bounds. The proposed controller is then constructed through backstepping technology to stabilize the closed-loop system. The validity is confirmed by extensively comparative experiments.

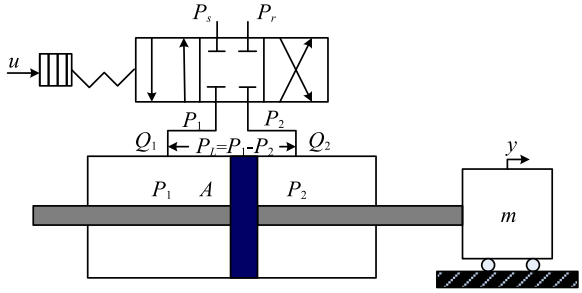


Fig. 1. Schematic diagram of a hydraulic system.

The rest of this article is arranged as follows. Section II establishes the hydraulic system model. The design of the controller and the stability analysis are presented in Section III. Section IV gives the experimental analysis. Finally, Section V concludes this article.

## II. Dynamic Models

In this article, as indicated in Fig. 1, a hydraulic system regulated by a servo valve is examined, and its load is driven by the hydraulic cylinder. Before establishing the system model, system parameters are defined as

The kinematic model of the system is described as follows:

$$\ddot{y} = \frac{A}{m}P_L - \frac{B}{m}\dot{y} + \frac{f_d(y,\dot{y},t)}{m} \tag{1}$$

where $f_d(y,\dot{y},t)$ indicates disturbances, including unmodeled nonlinear frictions, external disturbances, etc. The dynamic function of $P_L$ is established as reported in [21]

$$\frac{V_t}{4\beta_e}\dot{P}_L = -A\dot{y} - C_t P_L + q(t) + Q_L \tag{2}$$

where $q(t)$ is the modeling error, and $Q_L$ is modeled as [21]

$$Q_L = k_q x_v \sqrt{P_s - sign(x_v)P_L} \tag{3}$$

where $k_q = C_d w\sqrt{1/\rho}$ represents the flow gain. sign$(x_v)$ is defined by

$$\text{sign}(x_v) = \begin{cases} 1, & if\ x_v \geq 0 \\ -1, & if\ x_v < 0 \end{cases}. \tag{4}$$

Because of the high bandwidth of the servo valve, we neglect its dynamic characteristic and take $x_v$ as the proportional function of the control input $u$, i.e., $x_v = k_i u$, $k_i > 0$ is the gain coefficient.

Then, from (3), we have

$$Q_L = k_t u\sqrt{P_s - \text{sign}(u)P_L} \tag{5}$$

where $k_t = k_q k_i$.

Defining $x = [x_1, x_2, x_3]^T = [y, \dot{y}, AP_L/m]^T$, from (1)–(5), the state-space form can be reformulated by

$$\begin{aligned} \dot{x}_1 &= x_2 \\ \dot{x}_2 &= x_3 - \theta_1 x_2 + d_1(x,t) \\ \dot{x}_3 &= \theta_2 g(u, x_3)\, u - \theta_3 x_2 - \theta_4 x_3 + d_2(t) \end{aligned} \tag{6}$$

where $\theta_1 = B/m$, $\theta_2 = 4A\beta_e k_t/mV_t$, $\theta_3 = 4\beta_e A^2/mV_t$, $\theta_4 = 4\beta_e C_t/V_t$, $g(u, x_3) = \sqrt{P_s - m\text{sign}(u)x_3/A}$, $d_1(x, t) = f_d(x, t)/m$, and $d_2(t) = 4\beta_e Aq(t)/mV_t$.

*Assumption 1:* The parametric uncertainty $\theta = [\theta_1, \theta_2, \theta_3, \theta_4]^{\mathrm{T}}$, satisfies [40]

$$\boldsymbol{\theta} \in \boldsymbol{\Omega}_\theta = \{\theta : \|\theta\| \le \theta_M\} \tag{7}$$

where $\theta_M$ is a positive constant.

*Assumption 2:* The derivatives of the disturbances are bounded

$$\left|\dot{d}_1(x,t)\right| \le \delta, \left|\dot{d}_2(t)\right| \le \zeta \tag{8}$$

where $\delta > 0$ and $\zeta > 0$ are constants.

*Assumption 3:* The trajectory $x_{1d}(t)$ and its $i_{\text{th}}$ order derivatives $x_{1d}^{(i)}(t)$, $i = 1, 2, 3$, satisfy $x_{1d}(t) \le \upsilon_0 \le c_1 - \rho_0$ and $|x_{1d}^{(i)}(t)| \le \upsilon_i$. $\upsilon_0 > 0$, $c_1 > 0$, and $\upsilon_i > 0$ are constants, $\rho_0$ is given later.

## III. Controller Design and Stability Analysis

### A. Smooth Projection

To keep the parameter estimations within identified bounded sets, a smooth projection for the designed adaptive law is employed. In this article, $\hat{\bullet}$ indicates the estimation of $\bullet$ and $\tilde{\bullet} = \bullet - \hat{\bullet}$ denotes the estimation error. The smooth projection operator is described by [40]

$$\dot{\hat{\theta}} = \Pr oj_d(\phi, \hat{\theta}) = \phi - \frac{\zeta_1 \zeta_2}{4(\varsigma^2 + 2\varsigma\theta_M)^{n+1}\theta_M^2} \nabla p_d(\hat{\theta}) \tag{9}$$

where

$$\begin{aligned} p_d(\hat{\theta}) &= \hat{\theta}^T\hat{\theta} - \theta_M^2 \\ \zeta_1 &= \begin{cases} p_d^{n+1}(\hat{\theta}), & if\ p_d(\hat{\theta}) > 0 \\ 0, & \text{otherwise} \end{cases} \\ \zeta_2 &= \frac{1}{2}\nabla p_d(\hat{\theta})^T\phi + \sqrt{\left(\frac{1}{2}\nabla p_d(\hat{\theta})^T\phi\right)^2 + \kappa^2} \end{aligned} \tag{10}$$

where $\kappa > 0$, $\varsigma > 0$ are arbitrary constants. Then, we have following theorem.

*Theorem 1 [40]:* When $\hat{\theta}(0) \in \Omega_\theta$, the smooth projection operator assures that: (1)$\|\hat{\theta}(t)\| \le \theta_M + \varsigma\ \forall t \ge 0$; (2) $\tilde{\theta}^T \text{Proj}_d(\phi, \hat{\theta}) \ge \tilde{\theta}^T\phi$.

### B. Extended State Observer

After defining $x_{e2} = d_1(x, t)$, $x_{e3} = d_2(t)$, we construct ESOs for (6) as follows:

$$\begin{cases} \dot{\hat{x}}_1 = \hat{x}_2 + 3\omega_1(x_1 - \hat{x}_1) \\ \dot{\hat{x}}_2 = x_3 - \hat{\theta}_1 x_2 + \hat{x}_{e2} + 3\omega_1^2(x_1 - \hat{x}_1) \\ \dot{\hat{x}}_{e2} = \omega_1^3(x_1 - \hat{x}_1) \end{cases}$$

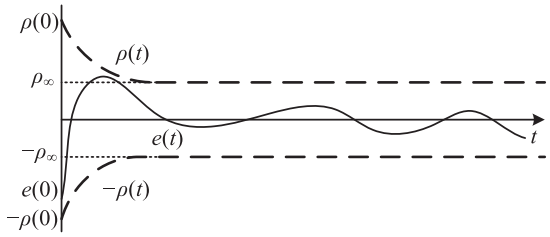


Fig. 2. Prescribed performance diagram.

$$\begin{cases} \dot{\hat{x}}_3 = \hat{\theta}_2 g(u, x_3)\, u - \hat{\theta}_3 x_2 - \hat{\theta}_4 x_3 + \hat{x}_{e3} + 2\omega_2(x_3 - \hat{x}_3) \\ \dot{\hat{x}}_{e3} = \omega_2^2(x_3 - \hat{x}_3) \end{cases} \tag{11}$$

where $\omega_1 > 0, \omega_2 > 0$ are the design parameters of the observer.

Let $\varepsilon_1 = [\varepsilon_{11}, \varepsilon_{12}, \varepsilon_{13}]^T = [\tilde{x}_1, \tilde{x}_2/\omega_1, \tilde{x}_{e2}/\omega_1^2]^T$, $\varepsilon_2 = [\varepsilon_{21}, \varepsilon_{22}]^T = [\tilde{x}_3, \tilde{x}_{e3}/\omega_2]^T$, we have

$$\begin{aligned} \dot{\varepsilon}_1 &= \omega_1 A_1 \varepsilon_1 - C_1\tilde{\theta}^T\varphi_2/\omega_1 + B_1 h_2(t)/\omega_1^2 \\ \dot{\varepsilon}_2 &= \omega_2 A_2 \varepsilon_2 - C_2\tilde{\theta}^T\varphi_3 + B_2 h_3(t)/\omega_2 \end{aligned} \tag{12}$$

where $\theta = [\theta_1, \theta_2, \theta_3, \theta_4]^T$, $\varphi_2 = [x_2, 0, 0, 0]^T$, $B_1 = [0, 0, 1]^T$, $\varphi_3 = [0, -g(u, x_3)u, x_2, x_3]^T$, $B_2 = [0, 1]^T$, $A_1 = \begin{bmatrix} -3 & 1 & 0 \\ -3 & 0 & 1 \\ -1 & 0 & 0 \end{bmatrix}$, $A_2 = \begin{bmatrix} -2 & 1 \\ -1 & 0 \end{bmatrix}$, $C_1 = [0, 1, 0]^T$, $C_2 = [1, 0]^T$, $h_2(t)$, and $h_3(t)$ are the derivatives of $d_1(x, t)$ and $d_2(t)$, respectively.

As $A_1$ and $A_2$ are Hurwitz matrices, we have $A_1^T P_1 + P_1 A_1 = -2I$ and $A_2^T P_2 + P_2 A_2 = -2I$ with positive definite matrices $P_1, P_2$.

### C. Prescribed Performance Function

Let $e(t) = x_1 - x_{1d}$ denotes the tracking error. To achieve the prescribed control performance, the tracking error $e(t)$ strictly satisfies the following inequality:

$$-\rho(t) < e(t) < \rho(t)\ \forall t > 0. \tag{13}$$

The strictly positive decreasing smooth PPF $\rho(t)$ is described by

$$\begin{aligned} \rho(t) &= (\rho_0 - \rho_\infty)\mathrm{e}^{-kt} + \rho_\infty \\ \lim_{t\to\infty} \rho(t) &= \rho_\infty > 0 \end{aligned} \tag{14}$$

where $\rho_0$, $\rho_\infty$, and $k$ are positive constants. As illustrated in Fig. 2, $\rho_0$ indicates the bound of the maximum overshoot, $k$ indicates the convergence rate, and the steady-state bound of $e(t)$ is constrained by $\rho_\infty$.

By choosing appropriate parameters of PPF, the control performance can be designed, and the transient performance can be enhanced to satisfy actual performance requirements.

### D. Controller Design

Let $z_2 = x_2 - \alpha_1$, $z_3 = x_3 - \alpha_2$. $\alpha_1$ and $\alpha_2$ are virtual controllers. The controller is developed as follows:

1) *Step 1:* A BLF is defined by

$$V_1 = \frac{1}{2}\log\frac{\rho^2(t)}{\rho^2(t)-e^2(t)} = \frac{1}{2}\log\frac{1}{1-z_1^2} \tag{15}$$

where $\log(\chi)$ is the natural logarithm of $\chi$, $z_1 = e(t)/\rho(t)$.

Differentiating $V_1$ and substituting (6) into its yields, we get

$$\dot{V}_1 = \frac{z_1\rho^{-1}}{1-z_1^2}\left(z_2+\alpha_1-\dot{x}_{1d}-\dot{\rho}z_1\right). \tag{16}$$

The virtual controller $\alpha_1$ is chosen as follows:

$$\alpha_1 = \dot{x}_{1d} - k_1 z_1 + \dot{\rho}z_1 \tag{17}$$

where $k_1 > 0$ denotes the feedback gain.

Then, $\dot{V}_1$ becomes

$$\dot{V}_1 = \frac{\rho^{-1}z_1z_2}{1-z_1^2} - \frac{\rho^{-1}k_1z_1^2}{1-z_1^2} \tag{18}$$

2) *Step 2:* Define BLF as

$$V_2 = \frac{1}{2}\log\frac{L_2^2}{L_2^2-z_2^2} + V_1 \tag{19}$$

where $L_2 > 0$ is a design parameter.

Then, we get $\dot{V}_2$ from (6) as follows:

$$\dot{V}_2 = \frac{z_2}{L_2^2-z_2^2}\left(z_3+\alpha_2-\theta_1x_2+d_1(x,t)-\dot{\alpha}_1\right)+\dot{V}_1. \tag{20}$$

The virtual controller $\alpha_2$ is specified as

$$\begin{aligned}\alpha_2 = {}& \hat{\theta}_1x_2 - \hat{x}_{e2} + \dot{\alpha}_1 - k_2z_2 \\ & - \frac{\rho^{-1}z_1\left(L_2^2-z_2^2\right)}{1-z_1^2} - \frac{\omega_1^4z_2}{2\left(L_2^2-z_2^2\right)}\end{aligned} \tag{21}$$

where $k_2 > 0$ is the feedback gain.

Then, we have

$$\begin{aligned}\dot{V}_2 = {}& \frac{z_2\left(\tilde{x}_{e2}-\tilde{\theta}_1x_2+z_3\right)}{L_2^2-z_2^2} - \frac{k_2z_2^2}{L_2^2-z_2^2} \\ & - \frac{\omega_1^4z_2^2}{2\left(L_2^2-z_2^2\right)^2} - \frac{\rho^{-1}k_1z_1^2}{1-z_1^2}.\end{aligned} \tag{22}$$

3) *Step 3:* Choose a BLF as

$$V_3 = \frac{1}{2}\log\frac{L_3^2}{L_3^2-z_3^2} + V_2 \tag{23}$$

where $L_3 > 0$ is a design parameter.

Then, we have $\dot{V}_3$ from (6) as

$$\begin{aligned}\dot{V}_3 = {}& \dot{V}_2 + \frac{z_3}{L_3^2-z_3^2}\left(\theta_2g(u,x_3)u-\theta_3x_2\right. \\ & \left.-\theta_4x_3+d_2(t)-\dot{\alpha}_2\right).\end{aligned} \tag{24}$$

The input $u$ is proposed as

$$\begin{aligned}u = {}& \frac{1}{\hat{\theta}_2g(u,x_3)} \\ & \times\begin{bmatrix}\hat{\theta}_3x_2+\hat{\theta}_4x_3-\hat{x}_{e3}+\dot{\alpha}_{2c}-\frac{L_3^2-z_3^2}{L_2^2-z_2^2}z_2-k_3z_3 \\ -\frac{z_3\left(\omega_2^2+\omega_1^4\left(\frac{\partial\alpha_2}{\partial x_2}\right)^2+\omega_1^2\left(\frac{\partial\alpha_2}{\partial x_1}\right)^2\right)}{2\left(L_3^2-z_3^2\right)}\end{bmatrix}\end{aligned} \tag{25}$$

where $k_3 > 0$ is a design parameter. $\dot{\alpha}_2 = \dot{\alpha}_{2c} + \dot{\alpha}_{2u}$, $\dot{\alpha}_{2c}$ denotes the calculable part, and $\dot{\alpha}_{2u}$ denotes the incalculable part.

$$\begin{aligned}\dot{\alpha}_{2c} = {}& \frac{\partial\alpha_2}{\partial t} + \frac{\partial\alpha_2}{\partial x_1}\hat{x}_2 + \frac{\partial\alpha_2}{\partial x_2}\dot{\hat{x}}_2 + \frac{\partial\alpha_2}{\partial\hat{x}_{e2}}\dot{\hat{x}}_{e2} + \frac{\partial\alpha_2}{\partial\hat{\theta}}\dot{\hat{\theta}} \\ & - \frac{\partial\alpha_2}{\partial x_2}3\omega_1^2\tilde{x}_1 \\ \dot{\alpha}_{2u} = {}& \frac{\partial\alpha_2}{\partial x_1}\tilde{x}_2 + \frac{\partial\alpha_2}{\partial x_2}\left(\tilde{x}_{e2}-\tilde{\theta}_1x_2\right).\end{aligned} \tag{26}$$

Then, we have

$$\begin{aligned}\dot{V}_3 = {}& -\frac{\rho^{-1}k_1z_1^2}{1-z_1^2} - \frac{k_2z_2^2}{L_2^2-z_2^2} - \frac{k_3z_3^2}{L_3^2-z_3^2} \\ & + \frac{z_2}{L_2^2-z_2^2}\left(\tilde{x}_{e2}-\tilde{\theta}_1x_2\right) \\ & - \frac{\omega_1^4z_2^2}{2\left(L_2^2-z_2^2\right)^2} + \frac{z_3}{L_3^2-z_3^2}\left(\tilde{x}_{e3}-\tilde{\theta}^T\varphi_3\right. \\ & \left.-\frac{\partial\alpha_2}{\partial x_1}\tilde{x}_2 - \frac{\partial\alpha_2}{\partial x_2}\left(\tilde{x}_{e2}-\tilde{\theta}_1x_2\right)\right) \\ & - \frac{\omega_2^2z_3^2}{2\left(L_3^2-z_3^2\right)^2} - \frac{\omega_1^4z_3^2}{2\left(L_3^2-z_3^2\right)^2}\left(\frac{\partial\alpha_2}{\partial x_2}\right)^2 \\ & - \frac{\omega_1^2z_3^2}{2\left(L_3^2-z_3^2\right)^2}\left(\frac{\partial\alpha_2}{\partial x_1}\right)^2.\end{aligned} \tag{27}$$

Utilizing Young's inequality, we obtain

$$\begin{aligned}\frac{z_2}{L_2^2-z_2^2}\tilde{x}_{e2} &\le \frac{\omega_1^4z_2^2}{2\left(L_2^2-z_2^2\right)^2} + \frac{\varepsilon_{13}^2}{2}, \\ \frac{z_3\tilde{x}_{e3}}{L_3^2-z_3^2} &\le \frac{\omega_2^2z_3^2}{2\left(L_3^2-z_3^2\right)^2} + \frac{\varepsilon_{22}^2}{2}, \\ -\frac{\partial\alpha_2}{\partial x_1}\frac{z_3\tilde{x}_2}{L_3^2-z_3^2} &\le \left(\frac{\partial\alpha_2}{\partial x_1}\right)^2\frac{\omega_1^2z_3^2}{2\left(L_3^2-z_3^2\right)^2} + \frac{\varepsilon_{12}^2}{2} \\ -\frac{\partial\alpha_2}{\partial x_2}\frac{z_3\tilde{x}_{e2}}{L_3^2-z_3^2} &\le \left(\frac{\partial\alpha_2}{\partial x_2}\right)^2\frac{\omega_1^4z_3^2}{2\left(L_3^2-z_3^2\right)^2} + \frac{\varepsilon_{13}^2}{2}.\end{aligned} \tag{28}$$

With (28), we have

$$\dot{V}_3 \le -\frac{\rho^{-1}k_1z_1^2}{1-z_1^2} - \frac{k_2z_2^2}{L_2^2-z_2^2} - \frac{k_3z_3^2}{L_3^2-z_3^2} - \frac{\tilde{\theta}^T\varphi_2z_2}{L_2^2-z_2^2}$$

$$+\frac{z_3}{L_3^2-z_3^2}\left(\tilde{\theta}^T\varphi_2\frac{\partial\alpha_2}{\partial x_2}-\tilde{\theta}^T\varphi_3\right)+\varepsilon_{13}^2+\frac{\varepsilon_{22}^2}{2}+\frac{\varepsilon_{12}^2}{2}. \tag{29}$$

### E. Stability Analysis

When the following conditions hold, Theorem 2 is performed to stabilize the closed-loop system.

1) Appropriate parameters $c_2$, $c_3$, $k_i$, $\omega_i$, and $L_i$ satisfy

$$c_2 \geq |\alpha_1|_{\max}+L_2, c_3 \geq |\alpha_2|_{\max}+L_3. \tag{30}$$

2) The initial conditions $z_i(0)$ meet

$$z(0)\in\mathbf{\Omega}_{z_0}\triangleq\{|z_1(0)|<1,|z_2(0)|<L_2,|z_3(0)|<L_3\}. \tag{31}$$

*Theorem 2:* With the proposed control law (25) and the following adaptation law, prescribed tracking performance is acquired with the nonviolation of full-state constraints. The boundedness of all signals is also guaranteed

$$\phi=\Gamma\left(\frac{z_3}{L_3^2-z_3^2}\left(-\varphi_3+\varphi_2\frac{\partial\alpha_2}{\partial x_2}\right)-\frac{\varphi_2 z_2}{L_2^2-z_2^2}\right)-\hat{\theta}. \tag{32}$$

where $\Gamma$ is a positive diagonal adaptation rate matrix.

Furthermore, the following positive definite Lyapunov function:

$$V_b=V_3+\frac{1}{2}\varepsilon_1^T P_1\varepsilon_1+\frac{1}{2}\varepsilon_2^T P_2\varepsilon_2+\frac{1}{2}\tilde{\theta}^T\Gamma^{-1}\tilde{\theta} \tag{33}$$

is bounded by

$$V_b(t)\leq\exp(-\lambda t)V_b(0)+\frac{\sigma}{\lambda}[1-\exp(-\lambda t)] \tag{34}$$

where $\lambda=\left\{2\rho_0^{-1}k_1,2k_2,2k_3,\frac{2\omega_1-5}{\lambda_{\max}(P_1)},\frac{2\omega_1-3}{\lambda_{\max}(P_2)},\left(2-\frac{\lambda_{\max}(\Gamma^{-1})}{\lambda_{\min}(\Gamma^{-1})}\right)\right\}_{\min}$, $\lambda_{\min}(\bullet)$ and $\lambda_{\max}(\bullet)$ are the minimum and the maximum eigenvalues of $\bullet$, respectively, $\sigma=\frac{\|P_1C_1\tilde{\theta}^T\varphi_2\|_{\max}^2}{2\omega_1^2}+\frac{\|P_1B_1\|^2\delta^2}{2\omega_1^4}+\frac{\|P_2C_2\tilde{\theta}^T\varphi_3\|_{\max}^2}{2}+\frac{\|P_2B_2\|^2\zeta^2}{2\omega_2^2}+\frac{1}{2}\lambda_{\max}(\Gamma^{-1})\|\theta\|^2$.

*Proof:* Differentiating $V_b$, substituting (12) and (29) into its yields, we have

$$\begin{aligned}\dot{V}_b\leq&-\frac{\rho^{-1}k_1z_1^2}{1-z_1^2}-\frac{k_2z_2^2}{L_2^2-z_2^2}-\frac{k_3z_3^2}{L_3^2-z_3^2}+\frac{-\tilde{\theta}^T\varphi_2z_2}{L_2^2-z_2^2}\\&+\frac{z_3}{L_3^2-z_3^2}\left(\tilde{\theta}^T\varphi_2\frac{\partial\alpha_2}{\partial x_2}-\tilde{\theta}^T\varphi_3\right)+\varepsilon_{13}^2+\frac{\varepsilon_{22}^2}{2}+\frac{\varepsilon_{12}^2}{2}\\&+\frac{1}{2}\left(\omega_1A_1\varepsilon_1-C_1\tilde{\theta}^T\varphi_2/\omega_1+B_1h_2(t)/\omega_1^2\right)^TP_1\varepsilon_1\\&+\frac{1}{2}\varepsilon_1^TP_1\left(\omega_1A_1\varepsilon_1-C_1\tilde{\theta}^T\varphi_2/\omega_1+B_1h_2(t)/\omega_1^2\right)\\&+\frac{1}{2}\left(\omega_2A_2\varepsilon_2-C_2\tilde{\theta}^T\varphi_3+B_2h_3(t)/\omega_2\right)^TP_2\varepsilon_2\\&+\frac{1}{2}\varepsilon_2^TP_2\left(\omega_2A_2\varepsilon_2-C_2\tilde{\theta}^T\varphi_3+B_2h_3(t)/\omega_2\right)-\tilde{\theta}^T\Gamma^{-1}\dot{\hat{\theta}}\end{aligned} \tag{35}$$

As $A_1^TP_1+P_1A_1=-2I$, $A_2^TP_2+P_2A_2=-2I$, we have

$$\begin{aligned}\dot{V}_b\leq&-\frac{\rho^{-1}k_1z_1^2}{1-z_1^2}-\frac{k_2z_2^2}{L_2^2-z_2^2}-\frac{k_3z_3^2}{L_3^2-z_3^2}-\frac{\tilde{\theta}^T\varphi_2z_2}{L_2^2-z_2^2}\\&+\frac{z_3}{L_3^2-z_3^2}\left(\tilde{\theta}^T\varphi_2\frac{\partial\alpha_2}{\partial x_2}-\tilde{\theta}^T\varphi_3\right)+\varepsilon_{13}^2+\frac{\varepsilon_{22}^2}{2}+\frac{\varepsilon_{12}^2}{2}\\&-\omega_1\|\varepsilon_1\|^2-\omega_2\|\varepsilon_2\|^2-\varepsilon_1^TP_1C_1\tilde{\theta}^T\varphi_2/\omega_1-\varepsilon_2^TP_2C_2\tilde{\theta}^T\varphi_3\\&-\varepsilon_1^TP_1B_1\frac{h_2(t)}{\omega_1^2}-\varepsilon_2^TP_2B_2\frac{h_3(t)}{\omega_2}-\tilde{\theta}^T\Gamma^{-1}\dot{\hat{\theta}}.\end{aligned} \tag{36}$$

With the adaptive law in (32), (36) becomes

$$\begin{aligned}\dot{V}_b\leq&-\frac{\rho^{-1}k_1z_1^2}{1-z_1^2}-\frac{k_2z_2^2}{L_2^2-z_2^2}-\frac{k_3z_3^2}{L_3^2-z_3^2}+\varepsilon_{13}^2+\frac{\varepsilon_{22}^2}{2}+\frac{\varepsilon_{12}^2}{2}\\&-\omega_1\|\varepsilon_1\|^2-\omega_2\|\varepsilon_2\|^2-\varepsilon_1^TP_1C_1\tilde{\theta}^T\varphi_2/\omega_1-\varepsilon_2^TP_2C_2\tilde{\theta}^T\varphi_3\\&-\varepsilon_1^TP_1B_1\frac{h_2(t)}{\omega_1^2}-\varepsilon_2^TP_2B_2\frac{h_3(t)}{\omega_2}-\tilde{\theta}^T\Gamma^{-1}\tilde{\theta}+\tilde{\theta}^T\Gamma^{-1}\theta.\end{aligned} \tag{37}$$

Utilizing Young's inequality, we get

$$\begin{aligned}-\varepsilon_1^TP_1C_1\tilde{\theta}^T\varphi_2/\omega_1&\leq\frac{1}{2}\|\varepsilon_1\|^2+\frac{\left\|P_1C_1\tilde{\theta}^T\varphi_2\right\|_{\max}^2}{2\omega_1^2}\\-\varepsilon_2^TP_2C_2\tilde{\theta}^T\varphi_3&\leq\frac{1}{2}\|\varepsilon_2\|^2+\frac{\left\|P_2C_2\tilde{\theta}^T\varphi_3\right\|_{\max}^2}{2}\\-\varepsilon_1^TP_1B_1\frac{h_2(t)}{\omega_1^2}&\leq\frac{1}{2}\|\varepsilon_1\|^2+\frac{\|P_1B_1\|^2|h_2(t)|_{\max}^2}{2\omega_1^4}\\-\varepsilon_2^TP_2B_2\frac{h_3(t)}{\omega_2}&\leq\frac{1}{2}\|\varepsilon_2\|^2+\frac{\|P_2B_2\|^2|h_3(t)|_{\max}^2}{2\omega_2^2}\\\tilde{\theta}^T\Gamma^{-1}\theta&\leq\frac{\lambda_{\max}(\Gamma^{-1})}{2\lambda_{\min}(\Gamma^{-1})}\tilde{\theta}^T\Gamma^{-1}\tilde{\theta}+\frac{\lambda_{\max}(\Gamma^{-1})}{2}\|\theta\|^2.\end{aligned} \tag{38}$$

Substituting (32) and (38) into (37), then we have

$$\begin{aligned}\dot{V}_b\leq&-\frac{\rho^{-1}k_1z_1^2}{1-z_1^2}-\frac{k_2z_2^2}{L_2^2-z_2^2}-\frac{k_3z_3^2}{L_3^2-z_3^2}-\left(\omega_1-\frac{5}{2}\right)\|\varepsilon_1\|^2\\&-\left(\omega_2-\frac{3}{2}\right)\|\varepsilon_2\|^2-\left(1-\frac{\lambda_{\max}(\Gamma^{-1})}{2\lambda_{\min}(\Gamma^{-1})}\right)\tilde{\theta}^T\Gamma^{-1}\tilde{\theta}+\sigma.\end{aligned} \tag{39}$$

As $\log\frac{L_j^2}{L_j^2-z_j^2}<\frac{z_j^2}{L_j^2-z_j^2}$ in the interval $z_j<L_j$ [32]. We have

$$\dot{V}_b\leq-\lambda V_b+\sigma. \tag{40}$$

Thus, (34) holds. As errors $z_i$, $\tilde{\theta}$, and $\tilde{\varepsilon}$ are bounded, the boundedness of $e(t)$ is guaranteed. Moreover, $\hat{\theta}$ and $\hat{x}_{ei}$ are bounded. As $x_1=e(t)+x_{1d}(t)$, $z_1=e(t)/\rho(t)$, and $|z_1|<1$with assumption 2, we get $|x_1|\leq c_1$, and $x_1$ is bounded. $\alpha_1$ in (17) is a function of $x_1$, $z_1$, and $\dot{x}_{1d}$. Due to the boundedness of $x_1$, $z_1$, and $\dot{x}_{1d}$, $\alpha_1$ is bounded. As $|x_2|\leq|\alpha_1|_{\max}+|z_2|$ and $|z_2|<L_2$, $|x_2|\leq c_2$ is got and $\alpha_2$ is bounded. Similarly, $|x_3|$ and $u$ are bounded.

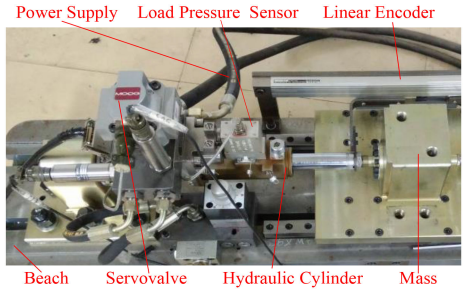


Fig. 3 Hydraulic system experimental table.

TABLE I
COMPONENTS AND SPECIFICATIONS

| Component | Specification |
|---|---|
| oil source pressure | 10 MPa |
| Servo valve | Moog G761-3003 |
| Efficient ram area of Hydraulic cylinder | 904.778 mm$^2$ |
| A/D card | Advantech PCI-1716 |
| High speed counter card | Heidenhain IK-220 |
| D/A card | Advantech PCI-1723 |
| Load mass | 30 kg |
| Pressure sensors | MEAS US175-C00002-200BG |
| Linear encoder | Heidenhain LC483 |

Therefore, the boundedness of all signals in the closed-loop system is guaranteed, the prescribed tracking performance is obtained, and all states are maintained in the constrained domain.

## IV. Experimental Results

### A. Experimental Platform

To verify the performance of the designed control method, an experimental platform demonstrated in Fig. 3 is built. Components and specifications are given in Table I. The system sampling time is 0.5ms. More details can be found in [25].

### B. Controllers for Comparison

The following four controllers are applied for comparison purposes to test the availability of the designed control strategy:

*1) ESOAPPC:* This is the extended-state-observer-based adaptive PPC with full-state constraints in (26). The controller parameters are tuned as: $k_1 = 1200$; $k_2 = 700$; $k_3 = 200$; $\Gamma = \text{diag}\{0.005,\ 3\times10^{-6},\ 1000,\ 0.02\}$; $\kappa = 10$, $\varsigma = 50$; $\theta_M = 8\times10^6$, $\omega_1 = 350$, $\omega_2 = 260$; and $\hat{\theta}(0) = [64, 9, 1\times10^6, 130]^T$. The parameters of PPF and BLF are shown in the analysis of experimental results.

*2) ESOAC:* This is the extended-state-observer-based adaptive controller same as the extended-state-observer-based adaptive PPC (ESOAPPC) but without the PPF and BLF. The parameters are the same as those in ESOAPPC.

*3) FLC:* This is the feedback linearization controller that is the same as the extended-state-observer-based adaptive controller (ESOAC) but without parameter adaptive estimation and disturbance compensations. The parameters are the same as those in ESOAC.

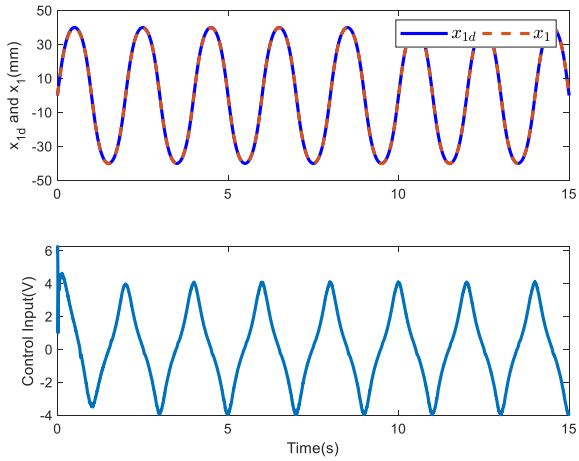


Fig. 4. Trajectory $x_{1\,d}$, output state $x_1$, and control input $u$.

TABLE II
THREE CONTROL PERFORMANCE INDICES OF FOUR CONTROLLERS

| Indexes | $M_e$ | $A_e$ | $S_\sigma$ |
|---|---|---|---|
| **FLC** | 0.6271 | 0.2843 | 0.1555 |
| **VFPI** | 0.3616 | 0.1847 | 0.1012 |
| **ESOAC** | 0.2535 | 0.1089 | 0.0759 |
| **ESOAPPC** | 0.1711 | 0.0659 | 0.0494 |

*4) VFPI:* Velocity feed-forward proportional-integral controller in [6] with P-gain $k_p = 3000$, I-gain $k_i = 700$, and velocity feed-forward gain $k_v = 28$ V·s/m.

*Remark 1:* Through the comparison of feedback linearization controller (FLC), velocity feed-forward proportional-integral controller (VFPI), and ESOAC, the effectiveness of adaptive law and disturbance compensation strategy can be certificated. Moreover, the effectiveness of state constrained control and prescribed tracking performance control can be proved by comparing ESOAC, VFPI, and ESOAPPC. In this way, the validity of ESOAPPC can be tested.

### C. Experimental Results and Discussion

The maximal absolute value ($M_e$), average value ($A_e$), and standard deviation ($S_e$) of tracking errors are employed to describe the control performance

$$M_e = \max_{i=1,\ldots,K}\{|e(i)|\},\ A_e = \frac{1}{K}\sum_{i=1}^{K}|e(i)|,$$
$$S_e = \sqrt{\frac{1}{K}\sum_{i=1}^{K}[|e(i)| - A_e]^2}. \tag{35}$$

where $K$ represents the number of the recorded digital signals.

1) *Case 1:* A trajectory $x_{1\,d} = 40\arctan(\sin(\pi t))/0.7854$ mm is first employed to verify the ability and applicability of the ESOAPPC. The PPF is set as $\rho(t) = (0.8 - 0.3)\mathrm{e}^{-2t} + 0.3$, $L_2 = 1$, $L_3 = 300$. Fig. 4 shows that the output state $x_1$ can accurately track $x_{1\,d}$ with a smooth and bounded control input $u$. The tracking errors and corresponding performance indices of the four controllers are presented in Table II and Fig. 5. Obviously, the

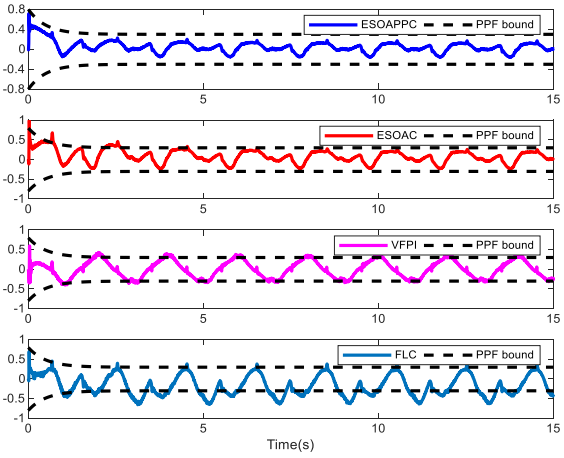


Fig. 5. Tracking errors $e(t)$ and PPF bound.

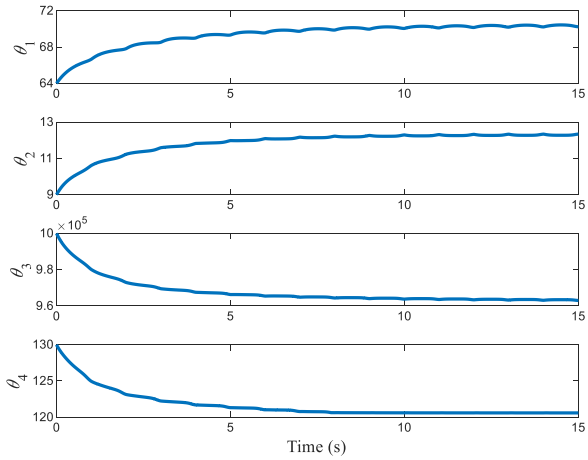


Fig. 6. Parameter adaptation of the ESOAPPC controller.

proposed ESOAPPC controller provides the best control performance. Moreover, the tracking error of ESOAPPC is retained within the PPF bound, while the prescribed performance constraints are violated by the other three controllers. Because ESOAPPC not only uses PPF to constrain tracking error but also combines ESO and adaptive algorithm to solve uncertainties to obtain better control performance. Fig. 6 presents the convergence of parameter estimation of ESOAPPC. They are all regular and bounded. Fig. 7 shows that $|z_1| < 1, |z_2| < L_2, |z_3| < L_3$, the full-state errors $z_1$, $z_2$, and $z_3$ are remained within the desired boundaries. Furthermore, system states are shown in Fig. 8. The full-state constraints can be assured.

2) *Case 2:* A fast smooth trajectory $x_{1d} = 20\arctan(\sin(4\pi t))/0.7854$ mm (see Fig. 9) is employed to further test the performance of the four controllers. The PPF is set as $\rho(t) = (1 - 0.4)\mathrm{e}^{-2t} + 0.4$, $L_2 = 1$, and $L_3 = 500$. The smooth trajectory $x_{1d}$ and output state $x_1$ are almost identical, and the control input $u$ is less than 10 V (see Fig. 9). The three indices of control performance are given in Table III, and the tracking errors are displayed in Fig. 10. As illustrated, better tracking accuracy is obtained by the ESOAPPC compared with the other three control

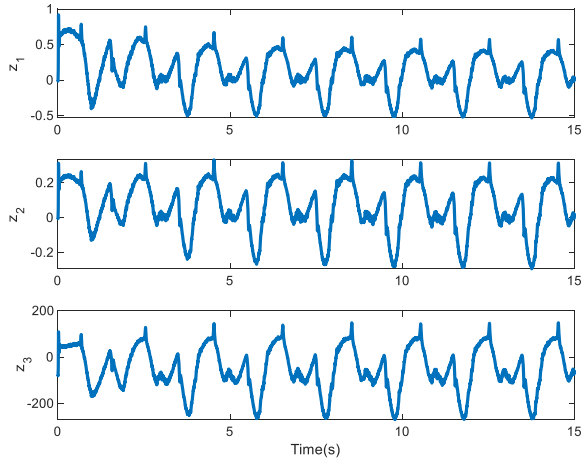


Fig. 7. Tracking errors $z_1$, $z_2$, and $z_3$.

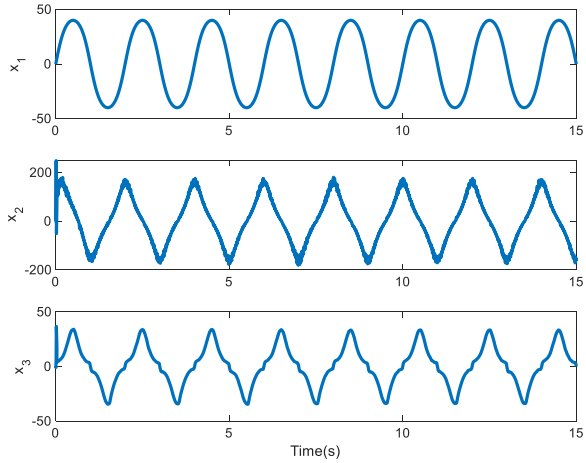


Fig. 8. System states $x_1$, $x_2$, and $x_3$.

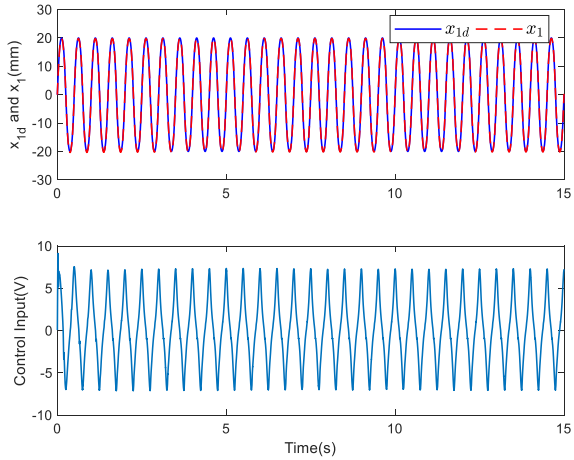


Fig. 9. Trajectory $x_{1d}$, output state $x_1$, and control input $u$.

TABLE III
THREE CONTROL PERFORMANCE INDICES OF FOUR CONTROLLERS

| Indexes | $M_e$ | $A_e$ | $S_\sigma$ |
|---|---|---|---|
| **FLC** | 1.1150 | 0.5100 | 0.3506 |
| **VFPI** | 0.6905 | 0.2610 | 0.1995 |
| **ESOAC** | 0.5222 | 0.1772 | 0.1424 |
| **ESOAPPC** | 0.3516 | 0.1313 | 0.0728 |

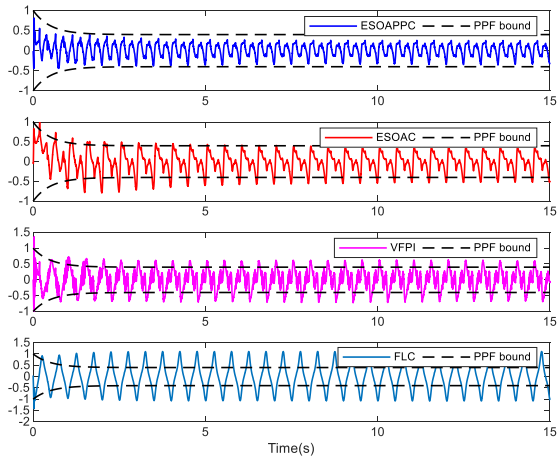


Fig. 10. Tracking errors $e(t)$ and PPF bound.

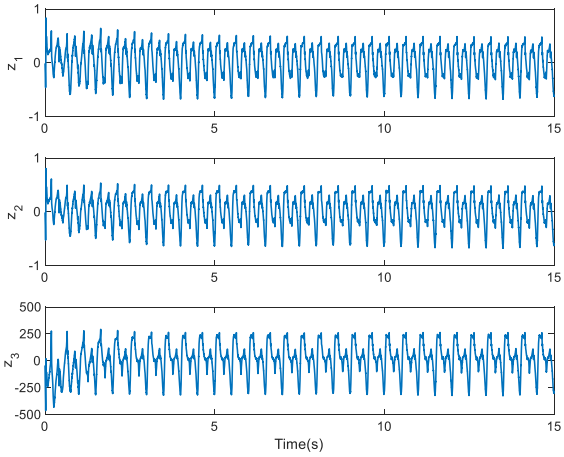


Fig. 11. Tracking errors $z_1$, $z_2$, and $z_3$.

methods. In addition, the tracking error of ESOAPPC is preserved within the PPF bound, which cannot be realized by the other three controllers. The reason is that the PPF is not utilized in the VFPI controller, FLC method and ESOAC scheme, so their tracking errors exceed the PPF bound. The full-state errors $z_1$, $z_2$, and $z_3$ are remained within the desirable boundaries (see Fig. 11), i.e., $|z_1| < 1, |z_2| < L_2, |z_3| < L_3$, the full-state constraints can be guaranteed. The system states are displayed in Fig. 12, and they are smooth and bounded.

3) *Case 3:* In this case, the four controllers are further tested for a low-frequency saw-tooth signal with an amplitude of 40 mm and a period of 2 s. The PPF is presented as $\rho(t) = (0.8 - 0.4)\mathrm{e}^{-2t} + 0.4$, $L_2 = 2.5$, and $L_3 = 320$. As presented in Table IV and Fig. 13, the proposed ESOAPPC algorithm ensures that the tracking error does not exceed the PPF bound and satisfactory tracking performance is achieved. Nevertheless, large transient and steady-state tracking errors are obtained by the other three controllers. The system states are demonstrated in Fig. 14. They are smooth and bounded. Experimental results prove that the proposed control method is effective under PPC and full-state constraints.

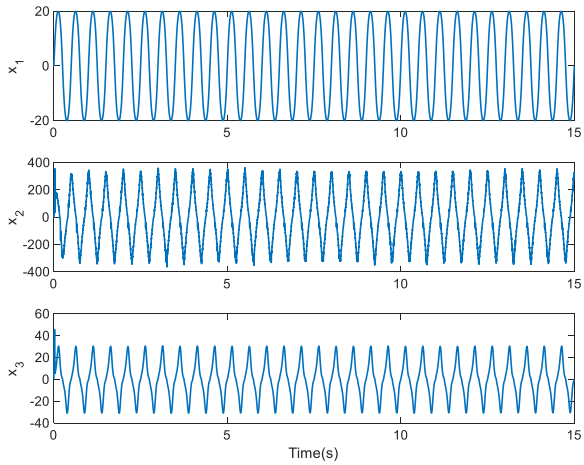


Fig. 12. System states $x_1$, $x_2$, and $x_3$.

TABLE IV
THREE CONTROL PERFORMANCE INDICES OF FOUR CONTROLLERS

| Indexes | $M_e$ | $A_e$ | $S_\sigma$ |
|---|---|---|---|
| **FLC** | 0.7716 | 0.6583 | 0.0797 |
| **VFPI** | 0.5375 | 0.2899 | 0.0959 |
| **ESOAC** | 0.4631 | 0.2165 | 0.0350 |
| **ESOAPPC** | 0.3371 | 0.1567 | 0.0217 |

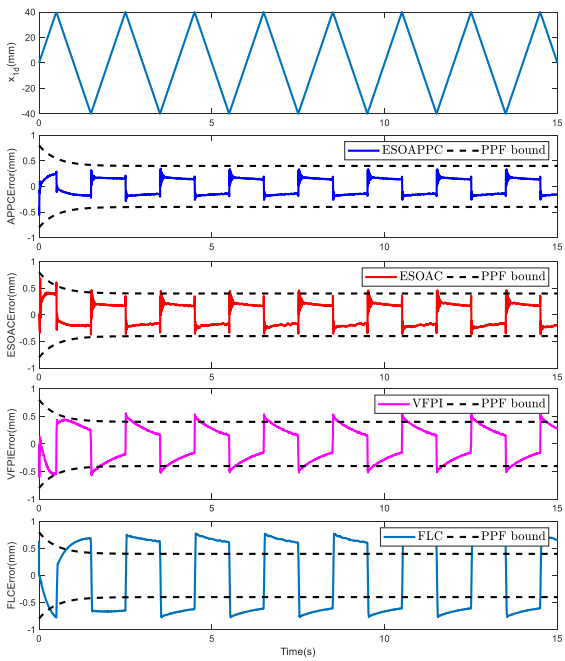


Fig. 13. Tracking errors $e(t)$ and PPF bound.

4) *Case 4:* A saw-tooth signal with a larger period is given to test the control performance. The PPF is set as $\rho(t) = (1 - 0.5)\mathrm{e}^{-2t} + 0.5$, $L_2 = 3$, and $L_3 = 360$. Table V and Figs. 15 and16 present the experimental results. From Table V and Fig. 15, one can see that only the proposed ESOAPPC can guarantee the tracking error to meet the prescribed performance demand. Furthermore, owing to the combination of ESO and adaptive control, the best

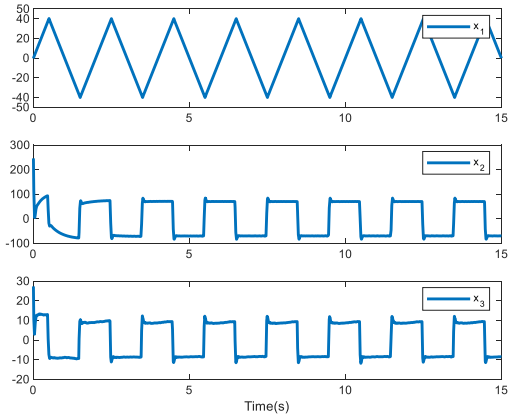


Fig. 14. System states $x_1$, $x_2$, and $x_3$.

TABLE V
THREE CONTROL PERFORMANCE INDICES OF FOUR CONTROLLERS

| Indexes | $M_e$ | $A_e$ | $S_\sigma$ |
|---|---|---|---|
| **FLC** | 0.8253 | 0.6184 | 0.1029 |
| **VFPI** | 0.6494 | 0.3810 | 0.0970 |
| **ESOAC** | 0.5312 | 0.1688 | 0.0498 |
| **ESOAPPC** | 0.3471 | 0.1442 | 0.0264 |

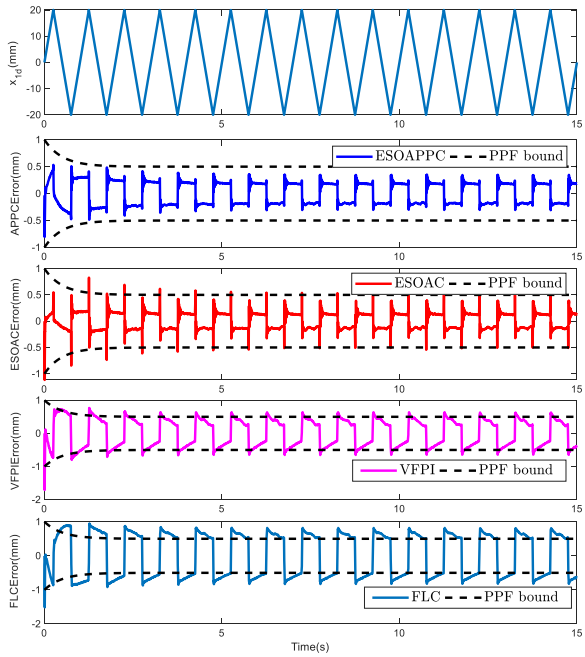


Fig. 15. Tracking errors $e(t)$ and PPF bound.

tracking performance is also achieved by the ESOAPPC. As shown in Fig. 16, the system states are also smooth and bounded.

5) *Case 5:* To detect the antidisturbance ability of the controller, an external disturbance $f = -4x_1$ is added to the system. A smooth trajectory $x_{1d} = 40 \arctan(\sin(\pi t))/0.7854$ mm is given to testify the ability and applicability of the proposed controller. The parameters of the PPF and BLF take the same values as the corresponding parameters in case 1. The tracking errors without and with disturbance are depicted in Fig. 17. One may find that satisfactory tracking performance is also achieved.

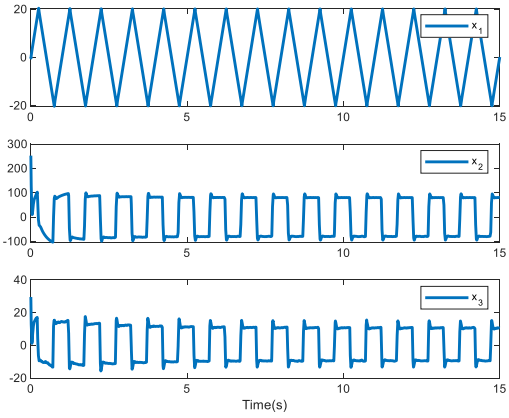


Fig. 16. System states $x_1$, $x_2$, and $x_3$.

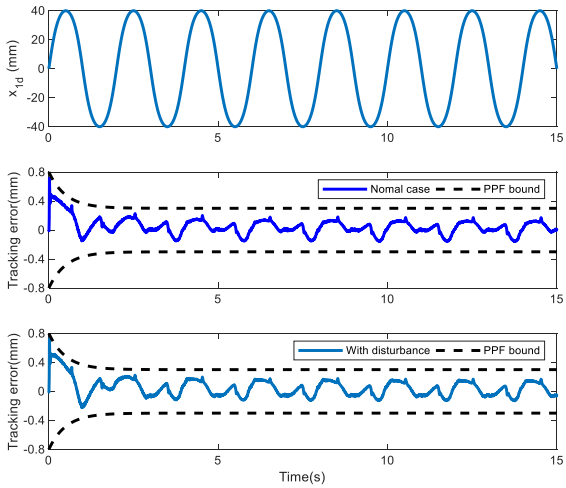


Fig. 17. Tracking errors $e(t)$ and PPF bound.

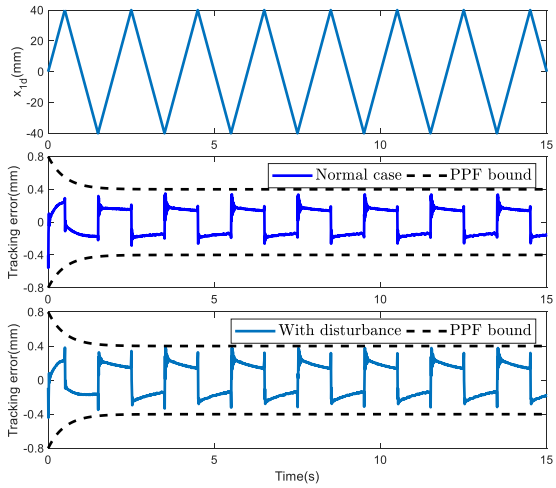


Fig. 18. Tracking errors $e(t)$ and PPF bound.

6) *Case 6:* Similar to the previous case, an external disturbance $f = -4x_1$ is added into the system. A low frequency saw-tooth signal with an amplitude of 40 mm and a period of 2 s is given. The parameters of the PPF and BLF are the same as those of Case 3. Fig. 18 depicts tracking errors without and with disturbance. It can be observed from Fig. 18 that all the tracking errors are retained within PPF bounds. Therefore, the control strategy is effective for uncertainties.

## V. Conclusion

This article presents an adaptive prescribed performance controller to keep the tracking errors and all states of hydraulic systems within predetermined ranges. The ESOs for estimating the disturbance and an adaptive law for estimating the unknown parameters are integrated to deal with the uncertainties of the system. Then the estimated uncertainties are brought into the controller. The transient behavior of tracking error and state errors within the expected boundary is assured by synthesizing the PPF and BLF. An adaptive prescribed performance controller with uncertainty compensation is performed to stabilize the closed-loop system. Finally, the control performance of the proposed controller is proved by numerous experimental results.

## References


[1] H. E. Merritt, *Hydraulic Control Systems*. New York, NY, USA: Wiley, 1967.

[2] J. Yao, Z. Jiao, D. Ma, and L. Yan, "High-accuracy tracking control of hydraulic rotary actuators with modeling uncertainties," *IEEE/ASME Trans. Mechatronics*, vol. 19, no. 2, pp. 633–641, Apr. 2014.

[3] B. Yao, F.P. Bu, J. Reedy, and G.T.C. Chiu, "Adaptive robust motion control of single-rod hydraulic actuators: Theory and experiments," *IEEE/ASME Trans. Mechatronics*, vol. 5, no. 1, pp. 79–91, Mar. 2000.

[4] C. Guan and S. Pan, "Nonlinear adaptive robust control of single-rod electro-hydraulic actuator with unknown nonlinear parameters," *IEEE Trans. Control Syst. Technol.*, vol. 16, no. 3, pp. 434–445, May 2008.

[5] W. Gu, J. Yao, Z. Yao, and J. Zheng, "Robust adaptive control of hydraulic system with input saturation and valve dead-zone," *IEEE Access*, vol. 6, pp. 53521–53532, 2018.

[6] Z. Xu, G. Qi, Q. Liu, and J. Yao, "ESO-based adaptive full state constraint control of uncertain systems and its application to hydraulic servo systems," *Mech. Syst. Signal Process*, vol. 167, 2021, Art. no. 08560.

[7] Q. Guo, J. Yin, T. Yu, and D. Jiang, "Saturated adaptive control of an electrohydraulic actuator with parametric uncertainty and load disturbance," *IEEE Trans. Ind. Electron.*, vol. 64, no. 10, pp. 7930–7941, Oct. 2017.

[8] J. Yao, W. Deng, and Z. Jiao, "Adaptive control of hydraulic actuators with Lugre model-based friction compensation," *IEEE Trans. Ind. Electron.*, vol. 62, no. 10, pp. 6469–6477, Oct. 2015.

[9] K.K. Ahn, D.N.C. Nam, and M. Jin, "Adaptive backstepping control of an electrohydraulic actuator," *IEEE/ASME Trans. Mechatronics*, vol. 19, no. 3, pp. 987–995, Jun. 2014.

[10] J. Yao, W. Deng, and W. Sun, "Precision motion control for electro-hydraulic servo systems with noise alleviation: A desired compensation adaptive approach," *IEEE/ASME Trans. Mechatronics*, vol. 22, no. 4, pp. 1859–1868, Aug. 2017.

[11] W. Deng, J. Yao, and D. Ma, "Robust adaptive precision motion control of hydraulic actuators with valve dead-zone compensation," *ISA Trans.*, vol. 70, pp. 269–278, Sep. 2017.

[12] Z. Yao, J. Yao, and W. Sun, "Adaptive RISE control of hydraulic systems with multilayer neural-networks," *IEEE Trans. Ind. Electron.*, vol. 66, no. 11, pp. 8638–8647, Nov. 2019.

[13] J. Yao, W. Deng, and Z. Jiao, "RISE-based adaptive control of hydraulic systems with asymptotic tracking," *IEEE Trans. Autom. Sci. Eng.*, vol. 14, no. 3, pp. 1524–1531, Jul. 2017.

[14] X. Dang, X. Zhao, C. Dang, H. Jiang, X. Wu, and L. Zha, "Incomplete differentiation-based improved adaptive backstepping integral sliding mode control for position control of hydraulic system," *ISA Trans.*, vol. 109, pp. 199–217, Mar. 2021.

[15] R. Fan and Y. Li, "An adaptive fuzzy trajectory tracking control via improved cerebellar model articulation controller for electro-hydraulic shovel," *IEEE/ASME Trans. Mechatronics*, vol. 26, no. 6, pp. 2870–2880, Dec. 2021.

[16] W. He, X. Mu, L. Zhang, and Y. Zou, "Modeling and trajectory tracking control for flapping-wing micro aerial vehicles," *IEEE/CAA J. Automat. Sinica*, vol. 8, no. 1, pp. 148–156, Jan. 2021.

[17] C. Sun, W. He, and J. Hong, "Neural network control of a flexible robotic manipulator using the lumped spring-mass model," *IEEE Trans. Syst., Man, Cybern. Syst.*, vol. 47, no. 8, pp. 1863–1874, Aug. 2017.

[18] F.P. Bu and B. Yao, "Desired compensation adaptive robust control of single-rod electro-hydraulic actuator," in *Proc. Amer. Control Conf.*, 2001, pp. 3926–3931.

[19] A. Mohanty and B. Yao, "Indirect adaptive robust control of hydraulic manipulators with accurate parameter estimates," *IEEE Trans. Control Syst. Technol.*, vol. 19, no. 3, pp. 567–575, May 2011.

[20] W. Sun, Z. Zhao, and H. Gao, "Saturated adaptive robust control for active suspension systems," *IEEE Trans. Ind. Electron.*, vol. 60, no. 9, pp. 3889–3896, Sep. 2013.

[21] J. Yao, Z. Jiao, and D. Ma, "Extended-state-observer-based output feedback nonlinear robust control of hydraulic systems with backstepping," *IEEE Trans. Ind. Electron.*, vol. 61, no. 11, pp. 6285–6293, Nov. 2014.

[22] Y. Li and L. He, "Counterbalancing speed control for hydrostatic drive heavy vehicle under long down-slope," *IEEE/ASME Trans. Mechatronics*, vol. 20, no. 4, pp. 1533–1542, Aug. 2015.

[23] W. He, T. Wang, X. He, L.-J. Yang, and O. Kaynak, "Dynamical modeling and boundary vibration control of a rigid-flexible wing system," *IEEE/ASME Trans. Mechatronics*, vol. 25, no. 6, pp. 2711–2721, Dec. 2020.

[24] D. Won, W. Kim, D. Shin, and C.C. Chung, "High-gain disturbance observer-based backstepping control with output tracking error constraint for electro-hydraulic systems," *IEEE Trans. Control Syst. Technol.*, vol. 23, no. 2, pp. 787–795, Mar. 2015.

[25] Z. Xu, D. Ma, J. Yao, and U. Nasim, "Feedback nonlinear robust control for hydraulic system with disturbance compensation," *Proc. Inst. Mech. Eng. Part I-J Syst. Control Eng.*, vol. 230, no. 9, pp. 978–987, Oct. 2016.

[26] W. Deng and J. Yao, "Extended-state-observer-based adaptive control of electrohydraulic servomechanisms without velocity measurement," *IEEE/ASME Trans. Mechatronics*, vol. 25, no. 3, pp. 1151–1161, Jun. 2020.

[27] J. Han, "From PID to active disturbance rejection control," *IEEE Trans. Ind. Electron.*, vol. 56, no. 3, pp. 900–906, Mar. 2009.

[28] C. Wang, L. Quan, Z. Jiao, and S. Zhang, "Nonlinear adaptive control of hydraulic system with observing and compensating mismatching uncertainties," *IEEE Trans. Control Syst. Technol.*, vol. 26, no. 3, pp. 927–938, May 2018.

[29] J. Yao and W. Deng, "Active disturbance rejection adaptive control of hydraulic servo systems," *IEEE Trans. Ind. Electron.*, vol. 64, no. 10, pp. 8023–8032, Oct. 2017.

[30] Q. Guo, Y. Zhang, B. G. Celler, and S. W. Su, "Backstepping control of electro-hydraulic system based on extended-state-observer with plant dynamics largely unknown," *IEEE Trans. Ind. Electron.*, vol. 63, no. 11, pp. 6909–6920, Nov. 2016.

[31] D. Won, W. Kim, and M. Tomizuka, "Nonlinear control with high-gain extended state observer for position tracking of electro-hydraulic systems," *IEEE/ASME Trans. Mechatronics*, vol. 25, no. 6, pp. 2610–2621, Dec. 2020.

[32] K. P. Tee, S. S. Ge, and E. H. Tay, "Barrier Lyapunov functions for the control of output-constrained nonlinear systems," *Automatica*, vol. 45, no. 4, pp. 918–927, Apr. 2009.

[33] W. He, Y. H. Chen, and Z. Yin, "Adaptive neural network control of an uncertain robot with full-state constraints," *IEEE Trans. Cybern.*, vol. 46, no. 3, pp. 620–629, Mar. 2016.

[34] Z. Li, J. Liu, Z. Huang, Y. Peng, H. Pu, and L. Ding, "Adaptive impedance control of human-robot cooperation using reinforcement learning," *IEEE Trans. Ind. Electron.*, vol. 64, no. 10, pp. 8013–8022, Oct. 2017.

[35] Q. Guo, Y. Zhang, B. G. Celler, and S. W. Su, "State-constrained control of single-rod electrohydraulic actuator with parametric uncertainty and load disturbance," *IEEE Trans. Control Syst. Technol.*, vol. 26, no. 6, pp. 2242–2249, Nov. 2018.

[36] C. P. Bechlioulis and G. A. Rovithakis, "Robust adaptive control of feedback linearizable MIMO nonlinear systems with prescribed performance," *IEEE Trans. Autom. Control,* vol. 53, no. 9, pp. 2090–2099, Oct. 2008.
[37] C. P. Bechlioulis and G. A. Rovithakis, "Adaptive control with guaranteed transient and steady state tracking error bounds for strict feedback systems," *Automatica*, vol. 45, no. 2, pp. 532–538, 2009.
[38] Q. Guo, Y. Zhang, B.G. Celler, and S.W. Su, "Neural adaptive backstepping control of a robotic manipulator with prescribed performance constraint," *IEEE Trans. Neural Netw. Learn. Syst.*, vol. 30, no. 12, pp. 3572–3583, Dec. 2019.
[39] Z. Xu, Q. Liu, and J. Yao, "Adaptive prescribed performance control for hydraulic system with disturbance compensation," *Int. J. Adapt. Control Signal Process*, vol. 35, no. 8, pp. 1544–1561, 2021.
[40] Z. Cai, M. S. Queiroz, and D. M. Dawson, "A sufficiently smooth projection operator," *IEEE Trans. Autom. Control*, vol. 51, no. 1, pp. 135–139, Jan. 2006.

**Zhangbao Xu** was born in Anhui Province, China, in 1988. He received B.S. degree in mechanical engineering and automation from Huaqiao University, Xiamen, China, in 2012, and the Ph.D. degree in mechanical engineering from the Nanjing University of Science and Technology, Nanjing, China, in 2017.

In 2017, he was a Lecturer with the School of Mechanical Engineering, Anhui University of Technology, Maanshan, China. His current research interests include high accuracy servo control of mechatronic systems, adaptive and robust control.

**Wenxiang Deng** received the B. Tech. degree in mechanical engineering from Central South University, Changsha, China, in 2013, and the Ph.D. degree in mechanical engineering from Nanjing University of Science and Technology, China, in 2018.

He is currently a Lecturer with the School of Mechanical Engineering, Nanjing University of Science and Technology, Nanjing, China. His current research interests include servo control of mechatronic systems, hydraulic robot control, robust adaptive control, and nonlinear compensation.

**Hao Shen** (Member, IEEE) received the Ph.D. degree in control theory and control engineering from Nanjing University of Science and Technology, Nanjing, China, in 2011.

From 2013 to 2014, he was a Postdoctoral Fellow with the Department of Electrical Engineering, Yeungnam University. Since 2011, he has been with Anhui University of Technology, China, where he is currently a Professor and a Ph.D. Supervisor. His current research interests include stochastic hybrid systems, complex networks, fuzzy systems and control, nonlinear control.

**Jianyong Yao** (Member, IEEE) was born in Shandong Province, China, in 1984. He received the B.Tech. degree in mechanical engineering and automation from the Tianjin University, Tianjin, China, in 2006, and the Ph.D. degree in mechatronics from the Beihang University, Beijing, China, in 2012.

In 2012, he was with the School of Mechanical Engineering, Nanjing University of Science and Technology, Nanjing, China, where he is currently a Professor. His current research interests include high accuracy servo control of mechatronic systems, adaptive and robust control, fault detection and accommodation of dynamic systems.